Results in Physics 64 (2024) 107921

Contents lists available at ScienceDirect

Results in Physics

journal homepage: www.elsevier.com/locate/rinp

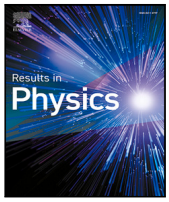

A rapid method for prediction of the non-resonant ultra-fast multipactor regime in high gradient RF accelerating structures

Daniel González-Iglesias [a,*], Benito Gimeno [a], Daniel Esperante [a,1], Pablo Martinez-Reviriego [a], Pablo Martín-Luna [a], Laura Karina Pedraza [a], Juan Carlos Fernández [a], Nuria Fuster-Martínez [a], Eduardo Martínez [a], Marçà Boronat [a], Alexej Grudiev [b]

[a] Instituto de Física Corpuscular (IFIC), CSIC-University of Valencia, c/ Catedrático José Beltrán 2, 46980 Paterna, Spain
[b] CERN, European Organization for Nuclear Research, Geneva 1221, Switzerland

ARTICLE INFO

Keywords:
Multipactor
Plasma discharge
RF particle accelerators
High gradient

ABSTRACT

The purpose of this work is to present an analytical method that allows to estimate in an approximate and fast way the presence of the non-resonant and ultra-fast multipactor effect in RF accelerating structures in the presence of high gradient electromagnetic fields. This single-surface multipactor regime, which has been little studied in the scientific literature, is characterised by appearing only under conditions of very strong RF electric fields (of the order of tens or hundreds of MV/m), where it is predominant over other types of single- or dual-surface resonance described in classical multipactor theory. This type of multipactor causes a rapid growth of the electron population and poses a serious drawback in the operation of RF accelerator components operating under high gradient conditions. Specifically, in dielectric-assist accelerating structures (DAA) it has been experimentally found that the presence of multipactor limits the maximum operating gradient of these components due to a significant increase in the reflected power due to the discharge, being this phenomenon the main problem to overcome. In a previous work, we found and described in detail by means of numerical simulations the presence of this non-resonant and ultra-fast multipactor regime in a DAA structure design for hadrontherapy. Here we aim to present a simple and fast method to predict the presence of this non-resonant and ultra-fast multipactor regime in RF accelerator structures with cylindrical revolution symmetry around the acceleration axis. This method is especially useful in the design stages of accelerating structures as it provides much faster results than numerical simulations of the multipactor, with quite good accuracy in a wide range of cases as shown in this paper.

Introduction

Multipactor discharge is an electron avalanche phenomenon that occurs in components operating under vacuum conditions and in the presence of high-power RF electromagnetic fields [1]. It can occur in a wide range of components, such as accelerator structures [2], passive component payloads of telecommunications satellites and klystrons. The multipactor effect occurs when the RF electric field accelerates the free electrons inside the device, pushing them towards the walls of the structure. When the electrons hit the walls, if their kinetic energy is in the appropriate range of the material, secondary electrons can be released from the surface, thus increasing the electron population inside the device. Provided a certain synchronism is established between the electrons and the RF electromagnetic field, this mechanism causes an exponential growth of the electron population leading to the breakdown of the multipactor. The onset of the discharge presents several drawbacks for the device performance, such as increased reflected power, heating of the device walls, outgassing, detuning of the resonant cavities, failure of the vacuum window and even physical damage to the surfaces.

To avoid these unwanted phenomena, the maximum operating RF power of the device must be reduced to levels where the absence of multipactor discharge is ensured. In order to design devices free from this RF breakdown phenomenon, numerous studies have been conducted on the multipactor effect in RF components. These studies aim to predict and understand the conditions necessary for the discharge to occur. In addition, possible methods to mitigate or suppress

* Corresponding author.
E-mail address: daniel.gonzalez-iglesias@uv.es (D. González-Iglesias).
[1] Also at Electronics Engineering Department, Universitat de València, 46100 Burjassot, Spain.

https://doi.org/10.1016/j.rinp.2024.107921
Received 10 April 2024; Received in revised form 24 July 2024; Accepted 12 August 2024
Available online 13 August 2024

the discharge, such as the application of secondary electron emission-reducing coatings on component surfaces or the application of external magnetic fields, are discussed.

Generally speaking, the classical multipactor theory described in [1] states that for a discharge to occur, there needs to be synchronicity between the electron trajectory and the RF electric field, and the impact kinetic energy of the electron needs to be in a favourable range to extract secondary electrons from the surface. Regarding the synchronisation between the electron and the RF electric field, this ensures that when the electron hits the surface, there is a polarity change in the RF electric field that pushes the electron away from the wall which it has just hit. This results in resonant trajectories that repeat periodically over time. Typically, these trajectories can be double-surface (if the electron alternately hits two different surfaces of the device) or single-surface (the electron always hits the same surface). The classical multipactor theory, developed for a metallic parallel-plate waveguide with a uniform time-harmonic RF electric field between the plates, establishes the times of flight between successive impacts of the electron with the component wall(s) that guarantee the resonance of the trajectories. In the case of double-surface multipactor, the time-of-flight must be an odd number of times the half-period of the RF signal (this half-period number is also known as the *order* of the multipactor). On the other hand, for the single-surface multipactor the time-of-flight must be an even number of times the half-period of the RF signal. Note that for single-surface multipactor to occur, the presence of a component of the RF electric field that is parallel to the surface, an electrostatic field perpendicular to the surface, or the presence of magnetic fields, is required. Of course, in the case of more complexes devices than a parallel-plate waveguide, these times of flight required for resonance between the electron and the electromagnetic field can vary to a greater or lesser extent, even leading to hybrid multipactor modes with more complex trajectories than those described above. In any case, this classical theory provides a good theoretical framework to interpret the multipactor phenomenology found in the results of the numerical simulations.

According to the above, the minimum time of flight between impacts that guarantees the resonance of the trajectories is an RF half-period and this occurs in the multipactor of a double surface. Therefore, if the electron trajectories had times of flight shorter than the RF half-period, resonance could not take place and the multipactor should not appear. As we increase the amplitude of the RF electric field, the time of flight between impacts of the electrons on the device decreases. Consequently, for very strong electromagnetic fields, the classical multipactor theory predicts the disappearance of the discharge. This fact can be seen, for example, in the Hatch and Williams curves [3], where the presence of an upper voltage limit at which multipactor discharge can occur is found.

Recently, in a study of the multipactor effect in new designs of accelerating dielectric structures intended for hadrontherapy [4], we observed in numerical simulations the presence of a multipactor regime that did not correspond to any of those studied in the scientific literature so far. Since this regime was characterised by the lack of a resonance condition between the RF electric field and the electron trajectory, we decided to call it non-resonant. Moreover, because the time between successive impacts with the component walls was much shorter than the half-period of the RF signal (which is the minimum limit set by classical multipactor theory for the discharge to occur), we applied the adjective ultra-fast to it. In addition, it should be noted that many successive impacts of the electron with the walls in a very short time also cause a very rapid growth in the electron population in the component, so this ultra-fast qualification also applies in this context. Precisely because this multipactor regime triggers the electron population in the component much faster than classical multipactor regimes, it makes this multipactor regime more damaging to device operation and tends to be predominant if present.

On the other hand, in our study of the dielectric-assist accelerating (DAA) structure we presented an approximate analytical model to understand on certain component-specific surfaces the new ultra-fast non-resonant regime found in simulations for high gradient operation, i.e., with very strong RF electric fields (of the order of tens and hundreds of MV/m). In this new work we have generalised the previous model to be able to describe approximately this multipactor regime in any wall of a cylindrical revolutionally symmetric RF accelerator device operating with high gradient RF electromagnetic fields. By applying the analytical equations of this model together with a detailed model of the secondary electron emission coefficient [5] (SEY, representing the average number of secondary electrons emitted per incident electron) of the surfaces we have developed a method to predict the risk of occurrence of an ultra-fast multipactor discharge in the device. This algorithm, which for brevity we will call MUNAMP (Method for Ultra-fast Non-resonant Analytical Multipactor Prediction), provides results with a fairly good accuracy in a wide range of cases as we will see in this article. Moreover, this method is much faster than the numerical simulations needed to analyse this type of devices. Therefore, MUNAMP is especially useful in the design stages of RF accelerator structures, being able to analyse a wide range of variants of the geometry and its dimensions, as well as SEY reducing materials or coatings, or even taking into account surface contamination (which is able to alter the SEY properties of the material), in an exceptionally fast time compared to any kind of numerical simulation of the device.

This paper is organised as follows. In Section b, the theoretical foundations of the method are described in detail and the equations of motion of the electron inside the accelerating cavity are solved approximately in an analytical manner. Section b explains how to apply the method to a general case. Then, in Section b, the results for several concrete examples of application of the method are shown and compared with the results obtained by accurate numerical simulations of the multipactor effect. The main conclusions of this study are presented in Section b. Finally, an appendix with step-by-step instructions for applying the MUNAMP method is included.

Theory

Let there be an RF accelerating cavity with cylindrical symmetry of revolution around the beam propagation axis, which we make coincide with the axis of a conventional cylindrical reference system z. Such a system can be properly described in cylindrical coordinates (r, ϕ, z), where r is the radial coordinate, ϕ the azimuthal angle and z the axial coordinate. Such cavities support electromagnetic modes of type TM_{0np}, which are typically used to accelerate the particle beam and are characterised by no dependence on the azimuthal angle [6]. Thus, the electromagnetic field at any position in the cavity can be expressed as follows:

$$\vec{E}_{RF}(\vec{r},t) = E_r(\vec{r},t)\hat{r} + E_z(\vec{r},t)\hat{z}; \qquad \vec{H}_{RF}(\vec{r},t) = H_\phi(\vec{r},t)\hat{\phi}$$

$$E_r = E_{0r}(r,z)\sin(\omega t+\theta)$$
$$E_z = E_{0z}(r,z)\sin(\omega t+\theta)$$
$$H_\phi = H_0(r,z)\cos(\omega t+\theta)$$

where $(\hat{r},\hat{\phi},\hat{z})$ are the unit vectors in the radial, azimuthal and axial directions, respectively, $\omega = 2\pi f$ is the angular frequency, f is the frequency, and θ is the initial phase of the electromagnetic field.

The differential equations governing the motion of the electron inside the cavity are obtained by equating the Lorentz force with Newton's Second Law. In the cases we are going to consider, it can be seen that the typical velocities are much smaller than the value of the speed of light in vacuum, so we will use the non-relativistic version of Newton's Second Law. Taking this into account the differential equations of motion can be expressed as

$$\begin{aligned}
\frac{dv_r}{dt} &= -\frac{e}{m}E_{0r}\sin(\omega t+\theta) + \frac{e}{m}\mu_0 H_0 v_z \cos(\omega t+\theta)\\
\frac{dv_\phi}{dt} &= 0\\
\frac{dv_z}{dt} &= -\frac{e}{m}\mu_0 H_0 v_r \cos(\omega t+\theta) - \frac{e}{m}E_{0z}\sin(\omega t+\theta)
\end{aligned} \tag{1}$$

where v_r, v_ϕ, v_z, are the radial, azimuthal and axial components of the velocity vector, respectively, e is the absolute value of the electron charge, and m is the electron mass.

We are interested in studying the trajectories of the electrons that generate the ultra-fast non-resonant multipactor regime. This type of multipactor is characterised by the fact that the electrons leave a certain position on the component walls and, after a time of flight much shorter than the period of the RF signal, they return to impact in a position very close to the starting position. In addition, because they have a very short time of flight, their maximum separation from the exit wall is very small. Because of this, we can approximate the electromagnetic field during the whole trajectory of the electron by its value at the exit position, a fact that allows us to simplify considerably the resolution of the differential equations of electron motion.

Suppose that the contour of the geometry of the accelerating cavity is described by the set of points $g = \{(z_l, r_l)\}$, where $l = 1, 2, \ldots, n_p$, and therefore the curve of the geometry can be approximated by $n_p - 1$ straight segments. Then we can define a pair of tangent $\hat{t}_k$ and normal $\hat{n}_k$ vectors for the kth segment which take the following expression

$$\begin{aligned} \hat{t}_k &= \alpha_k \hat{r} + \beta_k \hat{z} \\ \hat{n}_k &= -\beta_k \hat{r} + \alpha_k \hat{z} \end{aligned}$$
$$\alpha_k = \frac{\frac{\Delta r}{\Delta z}}{\sqrt{1 + \left(\frac{\Delta r}{\Delta z}\right)^2}}, \qquad \beta_k = \frac{1}{\sqrt{1 + \left(\frac{\Delta r}{\Delta z}\right)^2}}, \tag{2}$$

where $\Delta r = r_{k+1} - r_k$ and $\Delta z = z_{k+1} - z_k$. This coordinate system local to the surface formed by the vectors $(\hat{t}_k, \hat{n}_k)$ is more suitable to study the motion of the electrons in the cavity. We take the convention that the vector $\hat{n}_k$ always points to the vacuum inside the cell, so depending on the particular discretisation of the cavity profile, in some cases it may be necessary to reverse the vector $\hat{n}_k$ calculated with Eq. (2).

It can be easily seen that, according to the definition given by Eqs. (2), the vectors $(\hat{t}_k, \hat{n}_k)$ represent a rotation of the cylindrical coordinate axes $(\hat{r}, \hat{z})$. Therefore, we will make the identification $\cos\psi = \alpha_k$, $\sin\psi = \beta_k$, where ψ is the angle of rotation of the transformation between the two coordinate systems. It can be shown that the differential equations of electron motion in the new coordinate system is expressed as follows:

$$\begin{aligned} \frac{dv_t}{dt} &= -\frac{e}{m} E_{0t} \sin(\omega t + \theta) + \frac{e}{m} \mu_0 H_0 v_n \cos(\omega t + \theta) \\ \frac{dv_\phi}{dt} &= 0 \\ \frac{dv_n}{dt} &= -\frac{e}{m} \mu_0 H_0 v_t \cos(\omega t + \theta) - \frac{e}{m} E_{0n} \sin(\omega t + \theta) \end{aligned} \tag{3}$$

where v_t and v_n are the tangential and normal components of the velocity vector with respect to the local surface, respectively, while E_{0t} and E_{0n} are the tangential and normal components of the RF electric field, which are trivially calculated from the rotation of the cylindrical vector components as:

$$\begin{aligned} E_{0t} &= E_{0r} \cos\psi + E_{0z} \sin\psi \\ E_{0n} &= -E_{0r} \sin\psi + E_{0z} \cos\psi. \end{aligned} \tag{4}$$

The system of differential equations given by Eqs. (3) is analogous to that of eqs. (2) of [4]. However, in [4] these equations were only valid for a particular case of cavity wall orientation, whereas Eqs. (3) of this work are valid for an arbitrary wall orientation and thus for any accelerating cavity geometry as long as it has symmetry of revolution. In a similar way as in [4] it is possible to neglect in first approximation the term proportional to the magnetic field in the first equation of (3), since its contribution to the motion is weaker than the term proportional to the electric field. This approximation is valid since we are in the non-relativistic limit of electron motion [7] and makes it possible to simplify considerably the resolution of the tangential component of the velocity, which can be obtained by direct integration on both sides of the equality. Substituting the tangential velocity obtained in the differential equation of the normal coordinate, we can integrate and obtain both the normal velocity and, if we integrate again, the normal position. Finally, we arrive at the following equations for the velocity components and for the normal position:

$$v_t = v_{0t} + \frac{e}{m} \frac{E_{0t}}{\omega} \left[\cos(\omega t + \theta) - \cos\theta\right], \tag{5}$$

$$\begin{aligned} v_n =& v_{0n} + \frac{e}{m} \frac{E_{0n}}{\omega} \left[\cos(\omega t + \theta) - \cos\theta\right] \\ &+ \frac{e}{m} \frac{\mu_0 H_0}{\omega} \left[\frac{e}{m} \frac{E_{0t}}{\omega} \cos\theta - v_{0t}\right] \left[\sin(\omega t + \theta) - \sin\theta\right] \\ &+ \left(\frac{e}{2\omega m}\right)^2 \mu_0 E_{0t} \left[\sin(2\omega t + 2\theta) + 2\omega t - \sin(2\theta)\right], \end{aligned} \tag{6}$$

$$\begin{aligned} x_n =& x_{0n} + \left[v_{0n} - \frac{e}{m} \frac{E_{0n}}{\omega} \cos\theta - \frac{\xi'}{\omega} \sin\theta - \frac{\xi}{4\omega} \sin(2\theta)\right] t \\ &+ \frac{\xi}{4} t^2 + \frac{e}{m} \frac{E_{0n}}{\omega^2} \left[\sin(\omega t + \theta) - \sin\theta\right] \\ &- \frac{\xi'}{\omega^2} \left[\cos(\omega t + \theta) - \cos\theta\right] - \frac{\xi}{8\omega^2} \cos(2\omega t + 2\theta) \\ &+ \frac{\xi}{8\omega^2} \cos(2\theta), \end{aligned} \tag{7}$$

where v_{0t} and v_{0n} are the tangential and normal components of the electron release velocity from the surface, respectively, x_n is the normal coordinate with respect to the surface, and x_{0n} is the initial normal position at the instant of electron emission. In addition, we have defined the parameters $\xi \equiv \left(\frac{e}{m}\right)^2 \frac{\mu_0 H_0 E_{0t}}{\omega}$ and $\xi' \equiv \frac{e}{m} \mu_0 H_0 v_{0t} - \xi \cos\theta$.

If we assume that the time of flight t_i of the electron from its exit to its subsequent collision is very short ($t_i/T \ll 1$, where $T = 1/f$ is the RF period) then the normal coordinate of the trajectory can be approximated by using the Taylor series development of the sine and cosine functions present in Eq. (7) around the initial phase θ (see [4]) as:

$$x_n \approx x_{0n} + v_{0n} t + \frac{e}{2m} \left(\mu_0 H_0 v_{0t} \cos\theta - E_{0n} \sin\theta\right) t^2. \tag{8}$$

In the above equation by imposing that $x_n = x_{0n}$ we can estimate the impact time of the electron

$$t_i \approx \frac{v_{0n}}{\frac{e}{2m} \left(E_{0n} \sin\theta - \mu_0 H_0 v_{0t} \cos\theta\right)}. \tag{9}$$

From this expression we can obtain the minimum time of flight of the electron $t_{i,min}$ which occurs for the initial phase θ_{min},

$$\begin{aligned} t_{i,min} &= \frac{v_{0n}}{\frac{e}{2m} \sqrt{E_{0n}^2 + (\mu_0 H_0 v_{0t})^2}}, \\ \theta_{min} &= \arctan\left(\frac{E_{0n}}{\mu_0 H_0 v_{0t}}\right). \end{aligned} \tag{10}$$

Finally, the impact angle of the electron with respect to the normal to the surface ϑ_i is calculated as

$$\vartheta_i = \arccos\left(-\frac{v_n(t_i)}{\sqrt{v_n^2(t_i) + v_t^2(t_i)}}\right). \tag{11}$$

MUNAMP algorithm description

In this section we describe the MUNAMP method which, making use of the equations of the previous theoretical section. It allows us to estimate in an approximate and fast way the presence of the multipactor effect in the accelerating cavity. To begin with, we need to make a discretisation of the cavity profile (given by the set of points $g = \{(z_l, r_l)\}$) to assess the multipactor risk in the different regions of the structure described by the straight segments. Once this is done, we need to know the distribution of the RF electromagnetic field in the cavity. In this study, the influence of the polarisation electric field resulting from the emission or absorption of secondary electrons by the dielectric

surface is disregarded, as it has no significant impact in the initial stages of multipactor discharge growth [8,9]. In our case, we can obtain the RF electromagnetic field using the freely available electromagnetic software called SUPERFISH [10], which is especially useful and fast for accelerating structures that have symmetry of revolution. This software gives us the electric and magnetic field pattern on a two-dimensional grid in the coordinates (r, z). For our algorithm, we have to obtain the distribution of the fields at the previous points where we have discretised the cavity profile. This information is also straightforward to obtain in SUPERFISH if the cavity profile is provided as an external text file with the geometry points.

For each segment where we have discretised the cavity profile we estimate the multipactor risk as follows. First, we calculate both the minimum time between electron collisions ($t_{i,min}$) and the initial phase that satisfies this condition (θ_{min}) using Eqs. (10). In these expressions E_{0n} and E_{0t} are obtained from the amplitudes E_{0r} and E_{0n} using Eqs. (4). Here E_{0r}, E_{0z}, H_0 are proportional to the values of the RF electric and magnetic field amplitudes provided by SUPERFISH at the surface position that we are analysing. Regarding the initial electron velocity, we know that the kinetic energy spectrum of the emitted secondary electrons follows a distribution with a maximum at a few electron volts. In [11] the maximum emission probability is measured at 4.6 eV for platinum, while for dielectric materials in [12] we obtain measurements of the maximum in the range between $1.9 - 4.3$ eV depending on the particular material. According to this information, in our algorithm we will use an initial electron output kinetic energy of $W_0 = 4$ eV, since this value properly represents a typical secondary electron. Regarding the exit angle with respect to the surface normal, ϑ, secondary electrons follow a distribution known as the Cosine Law [13], whose maximum emission probability occurs at $\vartheta = 45°$. Because of this, we will choose this representative angle in our algorithm to calculate the initial components of the velocity vector ($v_{0n} = v_0 \cos\vartheta$, $v_{0t} = v_0 \sin\vartheta$, where $v_0 = \sqrt{2W_0/m}$). As discussed in the introduction, the ultra-fast non-resonant multipactor regime requires very high RF electric field amplitudes and very small inter-impact times. Therefore, the values of t_i obtained from Eq. (10) will not represent solutions compatible with this multipactor regime in all cases. Only if $t_i/T \ll 1$ the conditions for many successive impacts of the electron with the walls in a short time span are met, while maintaining the validity of the approximations used for the derivation of the t_i formula. More specifically, taking into account the results of numerical simulations for accelerating structures in which this type of multipactor [4] has been observed, we can establish empirically and in an approximate way that the maximum time between collisions that allows the appearance of this discharge regime is $\Gamma \equiv t_{max}/T = 0.05$. Therefore, if $t_{i,min}/T > \Gamma$ we have to rule out the possibility of multipactor existence at that surface position under these particular conditions. In case $t_{i,min}/T < \Gamma$, we substitute this impact time into Eqs. (5) and (6) to calculate the impact velocity, which in turn gives us the electron impact kinetic energy, W_i. As a consequence, Eq. (11) gives the electron impact angle. Knowing W_i and ϑ_i it is possible to obtain the value of the SEY in the collision, δ. There are different models that parameterise the SEY of a material, such as Vaughan's model [14] and Furman and Pivi model [15]. In our algorithm we will implement the Furman and Pivi model according to the equations presented in [16], because it is more complete than other models as it takes into account the different contributions to the total SEY (elastic collision, inelastic collision, and emission of true secondaries). However, it is worth mentioning that the MUNAMP method can be implemented with any other different SEY model without restrictions. In our particular case, once we have obtained the three contributions to the SEY according to the Furman and Pivi model, we add them together to obtain the total SEY of the impact. This is the value of the SEY that we have for an electron hitting the wall with the initial phase of the electromagnetic field that minimises the impact time. However, there may be other phases of the electromagnetic field that cause impact times below the limit set by Γ and, therefore, that are compatible with the presence of the multipactor regime we are looking for. To account for these other possibilities, we have to sweep the phases of the field around θ_{min}. For each θ phase considered in the scan we must now calculate the impact time using Eq. (9). Each t_i obtained must be filtered by eliminating those that do not satisfy the condition $t_i/T < \Gamma$. We will proceed by calculating the SEY in the manner described above for all those scan impact times that have satisfied the above condition. Having done this, we make the arithmetic mean of the SEY values obtained at this surface position, taking both the one obtained for the $t_{i,min}$ and the ones resulting from the phased scan. This average SEY value, δ_{avg}, is the essential information for determining the risk of an ultra-fast non-resonant multipactor discharge. The multipactor criterion for deciding that the discharger will occur is that $\delta_{avg} > 1$ [8,17]. Therefore, if at one or more positions on the surface of the accelerating cavity the above condition is satisfied, we can predict that the multipactor discharge will occur. A schematic summary of the algorithm presented in this section is given in the Appendix at the end of this document.

Application of the method in accelerating structures

In this section we will show the results obtained by applying the MUNAMP method for the prediction of the ultra-fast non-resonant multipactor effect in RF accelerating structures, comparing these results with accurate numerical simulations carried out with an in-house developed algorithm based on the Monte-Carlo [4] method.

The device we are going to analyse is a dielectric accelerator structure (DAA) cell designed for a linear accelerator of low-energy particles (such as protons or carbon ions) for hadrontherapy medical treatments. We will consider two different prototypes of the accelerator cell.

Prototype i

In this first prototype, the structure operates in the standing-wave regime with the $\pi - TM_{01}$ mode in S-band at a frequency of $f = 2999.42$ MHz. The schematic of the accelerator cell is shown in Fig. 1 (left) and has cylindrical symmetry of revolution around the z axis of beam propagation. The metal surrounding the cell is copper. The dielectric is $MgTiO_3$ with a relative dielectric permittivity of $\varepsilon_r = 16.66$. Typically, the dielectric is coated with a layer of SEY-reduced material in order to mitigate or inhibit the occurrence of multipactor discharge. In our case, we will test two types of coatings: 400 nm thick diamond-like carbon (DLC) coating applied by Nanotec Co. [18], and 400 nm amorphous carbon (aC) coating applied by CERN. In this work we will study the presence of multipactor in the case of the dielectric without coating and with the above two coatings. The main parameters of the SEY at normal incidence (first cross-over of the material or first energy at which the SEY is equal to unity W_1, energy at which the maximum SEY W_{max} is reached and value of the maximum SEY δ_{max}) are shown in Table 1 and have been obtained from experimental measurements [19].

In the DAA cell, the presence of multipactor has been analysed in the RF electric field amplitude range $E_0 \in [0.1, 200]$ MV/m, where E_0 represents the value of the maximum RF electric field in the axial axis of the structure. In the multipactor numerical simulations, the presence or absence of the discharge is determined for each value of E_0, in addition to the electron population growth factor σ, which is obtained by fitting the simulation data to the approximate theoretical expression $N_e(t/T) = N_0 e^{\sigma \frac{t}{T}}$, where N_e is the number of electrons, t is the time, and N_0 is the population at the initial time. The results of the numerical simulations are shown in Fig. 2 (a). For the estimation of the multipactor risk using the MUNAMP method, we sample the cell surface profile and, for each sample point, we obtain the average SEY δ_{avg} following the procedure described in Section b. If we find that $\delta_{avg} > 1$ in at least one point of the surface, we say that there is a risk of multipactor discharge. In Fig. 2 (b) the maximum value of the δ_{avg} found in the cavity (in cases where it is greater than unity) is

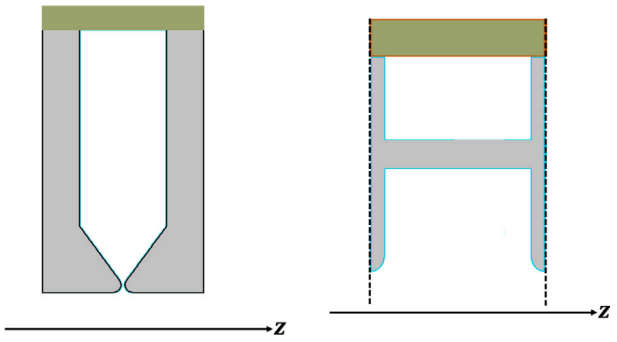

Fig. 1. Sketch of the cell of the DAA structure, on the left the first prototype and on the right the second prototype (the dielectric is shown in grey in both cases).

Table 1
Main SEY parameters.

Material	W_1 (eV)	W_{max} (eV)	δ_{max}
$MgTiO_3$ without coating	28.6	257.1	2.41
$MgTiO_3$ Nanotec Co. coating	66.6	291.7	1.69
$MgTiO_3$ ac-400 nm coating	225.5	428.0	1.07

Table 2
Prediction of multipactor in the DAA structure of prototype I according to the RF electric field amplitude E_0 expressed in MV/m.

	Uncoated	Nanotec Co. coat.	CERN coating
Simulations	0.1 – 200	0.1, 5 – 200	10 – 200
MUNAMP	0.6 – 200	3 – 200	6 – 200

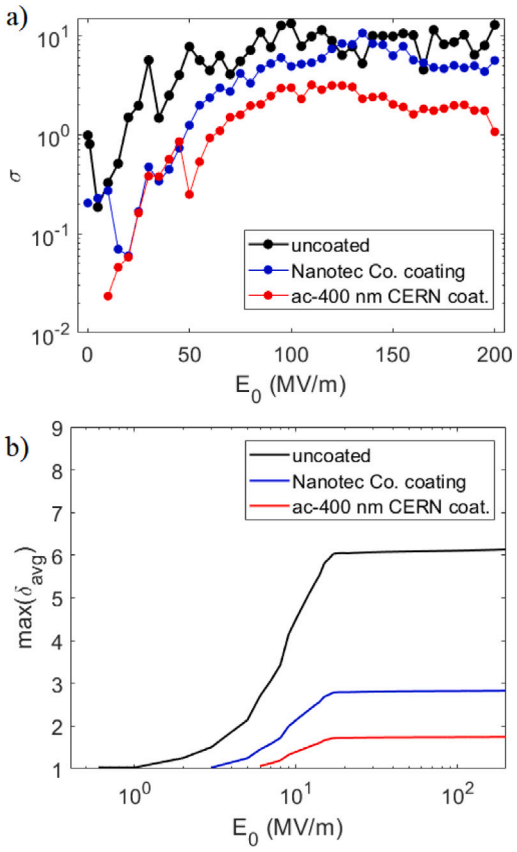

Fig. 2. Results for the DAA structure (prototype I): (a) for the numerical simulations, electron population growth factor as a function of RF electric field amplitude, (b) for the MUNAMP method, maximum value of the average SEY found on the surfaces of the structure as a function of the amplitude of the RF electric field.

plotted as a function of the electric field amplitude E_0. Similar to the growth factor σ obtained in the numerical simulations, the value of the maximum of δ_{avg} is indicative of the growth rate of the discharge. Both in the numerical simulations and in the results of the MUNAMP method shown in Fig. 2, it is obtained that the multipactor discharge grows faster in the uncoated dielectric case than in the cases with coatings. Furthermore, in both cases, the CERN ac−400 nm coating is found to inhibit the discharge growth the most. This is in agreement with the values of the SEY parameter W_1 shown in Table 1, where the highest value of W_1 is obtained for the CERN coating and the lowest value for the uncoated dielectric. It is interesting to summarise the results of Fig. 2 in the form shown in Table 2 in which the ranges of the RF electric field amplitude E_0 in which the multipactor discharge is found are indicated. As it can be seen, the E_0 ranges in which the MUNAMP method predicts the occurrence of the ultra-fast non-resonant multipactor match quite well with the accurate results of the numerical multipactor simulations for the cell with the three different materials analysed. Of course, the MUNAMP algorithm is an approximate method and cannot provide results as accurate as the numerical simulations. It should be mentioned that the inaccuracies in the estimation of the multipactor E_0 threshold value are due to the simplicity of the MUNAMP model, which is based on approximate equations of the electron dynamics and considers only a few trajectories of a standard electron to obtain results, unlike the numerical simulation algorithm based on the Monte-Carlo method which considers many electron trajectories in the cavity and with a precise resolution of the trajectories.

It is interesting to plot the mean value of the MUNAMP-estimated SEY δ_{avg} along the surface of the structure, information that indicates in which regions of the cavity the discharge is occurring. In Fig. 3 these results are shown as a colour map for the case of $E_0 = 15$ MV/m of the uncoated dielectric. According to the colour code (see caption of the figure), the ultra-fast non-resonant multipactor appears both at the bottom of the cavity dielectric and at the top in a region close to the corner of the structure. We can compare these results with the corresponding numerical simulations shown in Fig. 4. It should be mentioned that independent simulations have been performed launching in each case only electrons from the bottom or the top of the cavity, in order to study the possible differences in the multipactor phenomenology for each of these two areas of the cavity (in the simulations it is observed that the electrons do not cross from one region to the other). Figs. 4 (a) and (b) correspond to the upper region while subfigures (c) and (d) are for the lower region. The plots (a) and (c) are histograms in the form of a colour map showing the number of electrons hitting each point on the cavity surface and being able to release two or more secondary electrons. They therefore represent the regions where the multipactor effect occurs. In Fig. 4 (a) we see that in the upper region there is an area near the corners that contributes significantly to the discharge. Furthermore, this region agrees well with the prediction of the MUNAMP method for this part of the cavity shown in Fig. 3. Furthermore, in the lower region of the cavity, both the MUNAMP method and the simulations shown in Fig. 4 (c) predict multipactor effect. Figs. 4 (b) and (d) show the histogram with the electron times of flight between successive impacts with the surfaces for the numerical simulations, depending on whether the electrons are initially launched from the upper or the lower regions, respectively. The main maximum of the histogram is at $t_i/T = 0.03$ ($t_i/T = 0.007$) for the upper (lower) region. In both cases it is satisfied that the times of flight are less than the condition $t_i/T = \Gamma$ that we set as an upper limit to consider the presence of the ultra-fast non-resonant multipactor. Therefore, we have that in this analysed case this multipactor regime is the predominant one. However, taking another look at the histogram in Fig. 4 (b), we see that there are secondary maxima around $t_i/T = 2.5, 3.5, 4.5$. These secondary peaks are related to the presence of classical double-surface resonant multipactor regimes between the sidewalls of the upper part of the cavity.

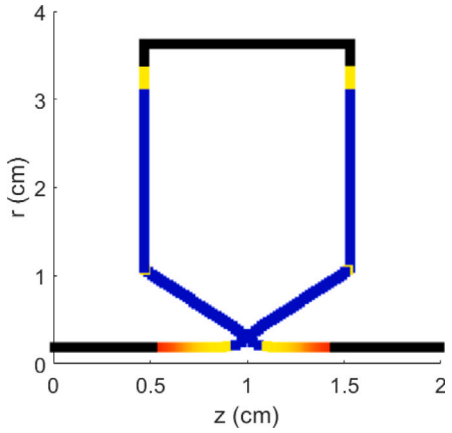

Fig. 3. Colour map with the average SEY (δ_{avg}) at the cavity surface (prototype I) obtained by the MUNAMP method for $E_0 = 15$ MV/m in the case of uncoated dielectric. The colour code is as follows: black if the conditions for ultra-fast trajectories are not met ($t_i/T > \Gamma$), blue if $\delta_{avg} < 1$, scale from yellow (when $\delta_{avg} = 1$) to red for $\delta_{avg} \geq 1$.

Prototype II

The second prototype of the DAA cell is the one previously discussed in another work by the authors [4]. The structure operates in the standing-wave regime with the $\pi - TM_{02}$ mode at a frequency of $f = 2998.1$ MHz. The dielectric material is identical to the one of the first prototype as are the coatings deposited on it. The geometry of the cell is shown in Fig. 1 (right). As we can see, there are two regions of the cell (down and up) which are separated by a dielectric wall so that the secondary electrons generated in one region cannot move to the other. Therefore, we will perform a separate multipactor study for each of the two regions of the cell. The results of the maximum value of the average SEY found on the surface of the structure, according to the MUNANP method, as a function of the RF electric field amplitude, are shown in Fig. 5. In addition, for a better interpretation of the results, the summary with the E_0 intervals where the multipactor discharge is expected is shown in Table 3. The results of the numerical simulations presented in [4] are also included. From the results we can see that, in most of the cases, there is a good agreement between the multipactor prediction of the MUNAMP method and the numerical simulations. There are only discrepancies in the cases of the down zone for the Nanotec Co. coating and for the down zone with the CERN coating.

In the case of the down zone with the Nanotec Co. coating, the difference in the multipactor prediction is due to the fact that in the range between 1 and 11 MV/m there is resonant multipactor but the conditions for the appearance of ultra-fast non-resonant multipactor do not exist. Indeed, if we examine the histogram with the time-of-flight between successive electron impacts with the device surfaces (see Fig. 6 left) we can see that for $E_0 = 5$ MV/m the typical times of flight are above the limit $t_i/T > \Gamma = 0.05$ (the main maximum of the distribution is around $t_i/T = 0.5$). By contrast, if we examine the same histogram for $E_0 = 15$ MV/m we observe that the situation has changed drastically, now the maximum of the histogram is around $t_i/T = 0.037$ and the times of flight are mostly below $t_i/T < \Gamma$, evidencing the emergence of the ultra-fast non-resonant multipactor as well as the disappearance of the classical multipactor regimes. Considering that the MUNAMP method only predicts non-resonant multipactor, the difference between the simulations and this method is justified.

Concerning the down zone with the CERN coating, we note that the simulations predict a series of multipactor bands for different electric field amplitude intervals (see Table 3), while the MUNAMP method gives a continuous discharge interval in 11 – 200 MV/m. Here the discrepancies are explained by the fact that we are close to the discharge inhibition limit due to the low SEY properties of the coating. This fact is responsible for the appearance of multipactor bands in the simulations,

Table 3
Prediction of multipactor in the DAA structure, prototype II according to the RF electric field amplitude E_0 expressed in MV/m.

	Simulations	MUNAMP
uncoated (down)	1–200	3–200
uncoated (up)	5–200	5–200
Nanotec Co. coat. (down)	1–200	11–200
Nanotec Co. coat. (up)	5–200	5–200
CERN coat. (down)	20–30, 50–60, 130–140, 170–200	12–200
CERN coat. (up)	10–200	11–200

alternating areas where discharge can occur with areas free of discharge. In the results of the maximum value of the average SEY found in the surfaces by the MUNAMP method (see Fig. 5), it is observed that in the whole multipactor range, the SEY values are very close to 1, being in the vast majority of cases below 1.1. Considering that MUNAMP is an approximate method, it is reasonable that in certain scenarios near the conditions separating the discharge and non-discharge cases, the prediction is not as accurate as the numerical simulations.

Similar to what was done for prototype I, we plot in Fig. 7 (a) and (c) the mean value of the SEY δ_{avg} estimated by MUNAMP along the surface of prototype II to highlight the regions where the discharge appears. The results are shown for the case of $E_0 = 20$ MV/m of the uncoated dielectric, for the upper and lower regions of the cavity. In addition, the results of the multipactor Monte-Carlo numerical simulations are also shown for comparison. Fig. 7(b) and (d) show the histograms in the form of a colour map showing the number of electrons that collide with each point on the cavity surface and are capable of releasing two or more secondary electrons (i.e., they represent the regions where the discharge grows). For the down zone, according to the MUNAMP results, the multipactor zone is located at the top of the sidewalls near the corners, with the maximum electron growth at the corner. A very slight production of secondaries is also predicted in a small area of the radial wall. If we compare the MUNAMP results with those of the numerical simulations, a good agreement is found: the main multipactor zone is the top of the sidewalls near the corner, and a minor emission of secondary electrons is also found in the radial wall. For the upper region of the cavity, the MUNAMP method finds the main multipactor zones in the radial wall near the lower left and lower right corners. In addition, a small region at the top of the sidewalls contributes slightly to the electron population increase. On the other hand, multipactor simulations predict that the main region of the discharge occurs in the radial wall near the lower left and lower right corners, agreeing well with the MUNAMP results. Also numerical simulations find a very slight electron production at other points on the sidewalls.

Finally, the speed of the MUNAMP method in obtaining results is noteworthy. The multipactor analysis of an accelerating structure with MUNAMP typically takes less than 1 s of computing time (on a standard PC computer with the algorithm implemented in MATLAB [20]) for each electric field amplitude value studied. On the other hand, a multipactor numerical simulation requires considerably longer times, which can vary quite a lot depending on the particular accelerating structure, but are generally around a few minutes. As an example, for the case of prototype II with $E_0 = 20$ MV/m, the numerical simulations took 4.5 min. Taking into account that in order to analyse the multipactor effect on a structure, many values of E_0 have to be considered, the time difference between simulation and MUNAMP method becomes more significant. Moreover, as seen in the previous results, the presence of the multipactor effect is typical in many accelerating structures and this poses a problem in their operation. Therefore, it is important to try to design multipactor-free devices or to reduce the impact of this phenomenon as much as possible. This requires testing multiple geometries and/or coatings. In this sense, the MUNAMP method has a great advantage over numerical simulations in the design stages of the device, allowing many different prototypes to be analysed in a much shorter time. However, it must be remarked that the method described in this

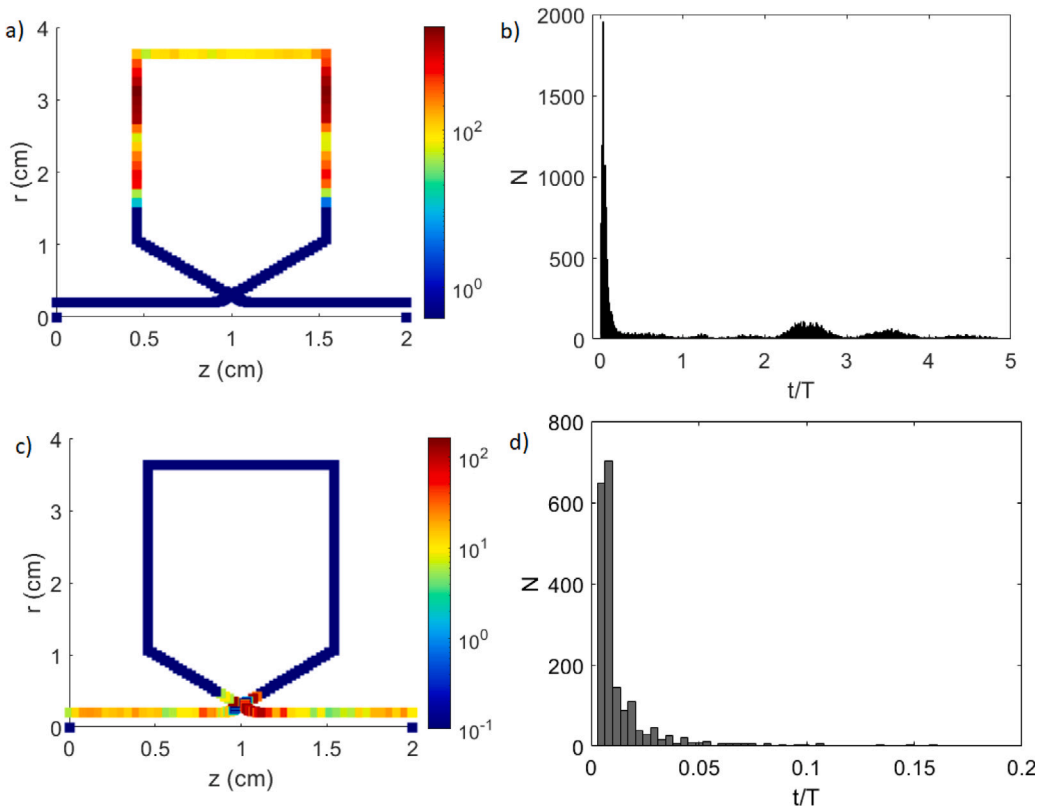

Fig. 4. Statistics of the multipactor numerical simulations for $E_0 = 15$ MV/m in prototype I. (a) Histogram in the form of a colour map with the number of electrons that impact on each portion of the surface and are capable of releasing two or more secondary electrons, for a simulation with initial electrons launched only from the upper region of the cavity. (b) Histogram with the times of flight of the electrons between successive impacts with the surfaces, for electrons launched initially from the upper region of the cavity. Figures (c) and (d) are analogous to figures (a) and (b) changing that electrons are launched initially from the lower region instead from the upper region.

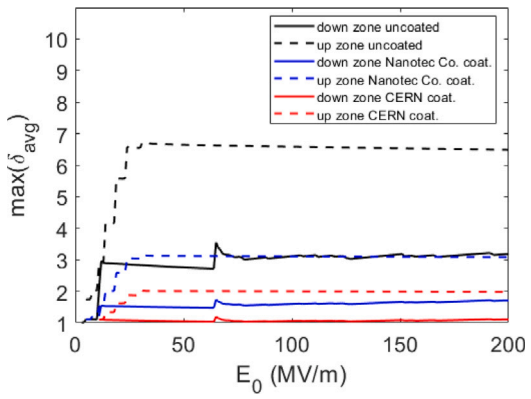

Fig. 5. Results for the DAA structure (prototype II) with the MUNAMP method: maximum value of the average SEY found on the surfaces of the structure as a function of the amplitude of the RF electric field.

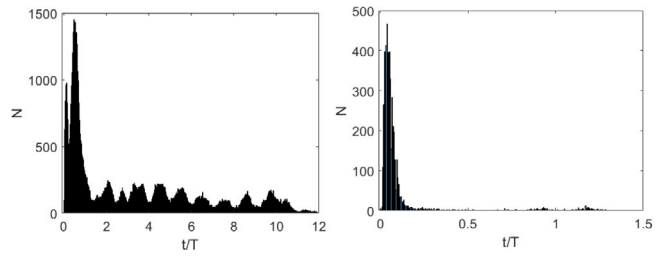

Fig. 6. Histogram showing the electron times of flight between successive impacts with the surfaces as a function of normalised time, for prototype II with the Nanotec Co. coating in the down zone (left $E_0 = 5$ MV/m, right $E_0 = 15$ MV/m).

manuscript is intended to provide a quick approximation of the multipactor behaviour of the device, but of course it will not be as accurate as proper 3D numerical simulations with a Monte-Carlo algorithm.

Conclusions

In this work we have presented an approximate method, which we have called MUNAMP, for the prediction of the non-resonant and ultra-fast multipactor effect in RF accelerator structures in the presence of high gradient RF electromagnetic fields. This method is based on analytical approximations of the equations of motion of the electron inside the device and it is applicable to any accelerator structure with cylindrical symmetry of revolution around the propagation axis of the particle beam. After describing the MUNAMP algorithm in detail, we have applied the method to two designs of dielectric accelerator structures, obtaining the amplitude ranges of the RF electric field in which the multipactor discharge occurs. These results have been compared with numerical simulations of a Monte-Carlo code developed by ourselves to study the multipactor effect in this type of structures. The comparison between the results of the simulations and MUNAMP is good, showing that this method is able to make an approximate prediction of the RF electric field amplitudes at which the discharge occurs. A strength of the MUNAMP method is that it is much faster computationally than the conventional numerical simulations, though it is, of course, not as accurate as these simulations. This fact makes this method especially useful in the design stages of accelerator structures, as it allows estimating the risk of multipactor discharge in a much shorter time than numerical simulations, allowing many variants of the geometry and/or coatings to be analysed, thus optimising the design to try to prevent the occurrence of the discharge.

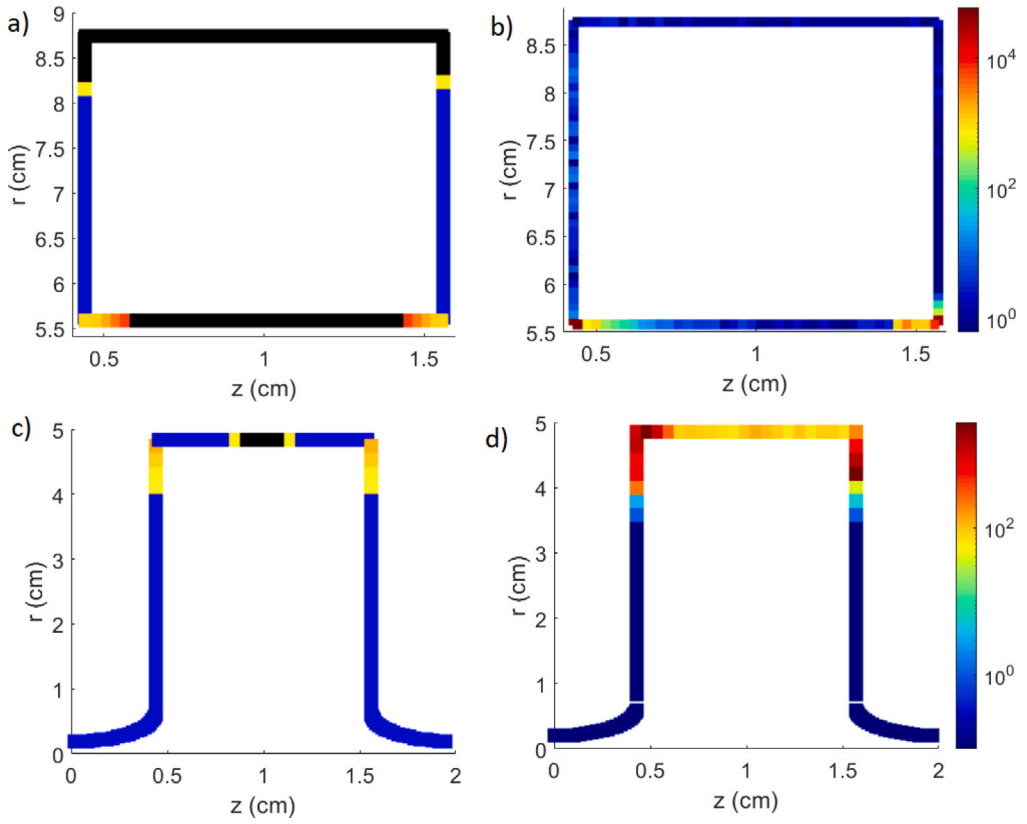

Fig. 7. Comparison between the MUNAMP method and the numerical simulations for $E_0 = 20$ MV/m in prototype II with the uncoated dielectric. (a) and (c) are the colour maps with the average SEY (δ_{avg}) at the cavity surface of the up and down zones, respectively. The colour code is as follows: black if the conditions for ultra-fast trajectories are not met ($t_i/T > \Gamma$), blue if $\delta_{avg} < 1$, scale from yellow (when $\delta_{avg} = 1$) to red for $\delta_{avg} \geq 1$. (b) and (d) are the histograms in the form of a colour map with the number of electrons that impact on each portion of the surface and are capable of releasing two or more secondary electrons, for the up and down zones, respectively.

CRediT authorship contribution statement

Daniel González-Iglesias: Writing – original draft, Validation, Software, Methodology, Investigation, Formal analysis, Conceptualization. **Benito Gimeno:** Writing – review & editing, Supervision, Resources, Project administration, Funding acquisition, Conceptualization. **Daniel Esperante:** Writing – review & editing, Supervision, Resources, Project administration, Funding acquisition, Conceptualization. **Pablo Martinez-Reviriego:** Writing – review & editing. **Pablo Martín-Luna:** Writing – review & editing, Conceptualization. **Laura Karina Pedraza:** Writing – review & editing. **Juan Carlos Fernández:** Writing – review & editing, Conceptualization. **Nuria Fuster-Martínez:** Writing – review & editing. **Eduardo Martínez:** Writing – review & editing. **Marçà Boronat:** Writing – review & editing. **Alexej Grudiev:** Writing – review & editing.

Declaration of competing interest

The authors declare that they have no known competing financial interests or personal relationships that could have appeared to influence the work reported in this paper.

Data availability

Data will be made available on request.

Acknowledgments

This work was supported by the Ministerio de Ciencia e Innovación of the Spanish Government under Grant PTA2020-019613-I, Grant FPU20/04958, and Grant FPU19/00585.

Summary of the munamp algorithm

The MUNAMP algorithm for the estimation of the risk of a non-resonant ultra-fast multipactor discharge can be summarised in the following steps:

1. Discretisation of the cylindrical cavity profile in a set of points $g = \{(z_l, r_l)\}$ and their corresponding segments in order to analyse the surface.
2. Calculation of the RF electric and magnetic fields at the sampled points and segments, using electromagnetic software such as SUPERFISH.
3. Select a (new) sampled segment of the surface.
4. For such a segment, calculate the minimum impact time $t_{i,min}$ and its corresponding initial phase θ_{min} using Eqs. (10).
5. If $t_{i,min}/T > \Gamma$ discard the presence of multipactor at that surface position and go back to step 3. Otherwise continue with the next step.
6. We substitute $t_{i,min}$ and θ_{min} into Eqs. (5) and (6) in order to calculate the impact velocity, then obtain electron impact kinetic energy, W_i.
7. Using Eq. (11) we obtain the electron impact angle ϑ_i.
8. We calculate the SEY, δ from W_i and ϑ_i. The particular equations will depend on the SEY model that we have chosen. We save the value of δ obtained.
9. We sample the phases of the electromagnetic field in an interval centred on θ_{min} taking values $\theta_k = 1, 2, \ldots, N_k$.
10. We take a (new) value of the sampling θ_k and use Eq. (9) to calculate the impact time t_i.
11. If $t_i/T > \Gamma$ we discard a value of θ_k and go back to the previous step. Otherwise, we continue to the next step.

12. We repeat steps 6 to 8 but using t_i and θ_k instead of $t_{i,min}$ and θ_{min}.
13. We go back to step 10 until we have analysed N_k samples of θ_k.
14. We take the arithmetic mean of the N_k values of the SEY corresponding to the sampling of the initial phase δ_{avg}, without forgetting to include the value of δ corresponding to θ_{min}.
15. If $\delta_{avg} > 1$ then we consider that at the analysed position of the surface we will have ultra-fast non-resonant multipactor. Otherwise we do not expect discharge.
16. We return to the step 3 until the analysis of all the sampled segments of the cavity is completed.

In Fig. .8 is shown the flowchart of the MUNAMP algorithm.

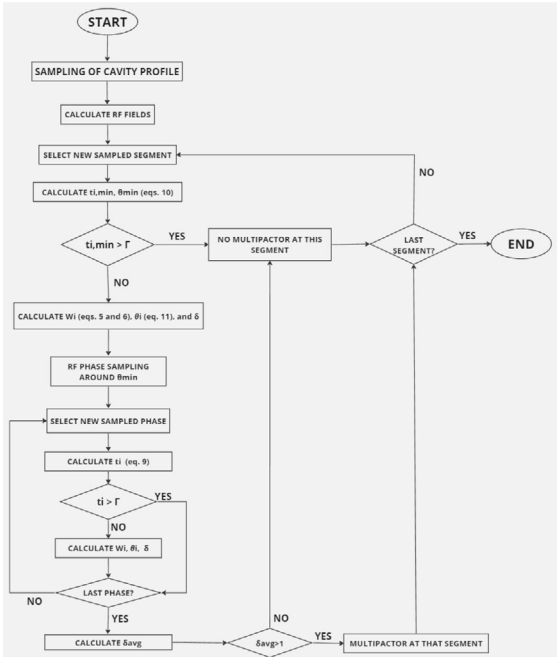

Fig. .8. Flowchart of the MUNAMP algorithm.

References

[1] Vaughan J. Multipactor. IEEE Trans Electron Devices 1988;35(7):1172–80.
[2] Shemelin VD, Belomestnykh SA. Multipactor in Accelerating Cavities. Switzerland: Springer; 2020.
[3] Hatch AJ, Williams HB. Multipacting modes of high-frequency gaseous breakdown. Phys Rev 1958;112:681–5.
[4] González-Iglesias D, Gimeno B, Esperante D, Martinez-Reviriego P, Martín-Luna P, Fuster-Martínez N, et al. Non-resonant ultra-fast multipactor regime in dielectric-assist accelerating structures. Results Phys 2024;56:107245.
[5] Reimer L. Scanning electron microscopy. In: Springer series in optical sciences.
[6] Wangler TP. RF linear accelerators. John Wiley & Sons, Ltd; 2008.
[7] Semenov VE, Rakova EI, Anderson D, Lisak M, Puech J. Multipactor in rectangular waveguides. Phys Plasmas 2007;14(3):033501.
[8] Coves A, Torregrosa-Penalva G, Vicente C, Gimeno B, Boria VE. Multipactor discharges in parallel-plate dielectric-loaded waveguides including space-charge effects. IEEE Trans Electron Devices 2008;55(9):2505–11.
[9] Torregrosa G, Coves A, Vicente C, Perez A, Gimeno B, Boria V. Time evolution of an electron discharge in a parallel-plate dielectric-loaded waveguide. IEEE Electron Device Lett 2006;27(7):619–21.
[10] Halbach K, Holsiger RF. SUPERFISH - a computer program for evaluation of RF cavities with cylindrical symmetry. Part Accel 1976;7:213–22.
[11] Bronchalo E, Coves A, Mata R, Gimeno B, Montero I, Galán L, et al. Secondary electron emission of pt: Experimental study and comparison with models in the multipactor energy range. IEEE Trans Electron Devices 2016;63(8):3270–7.
[12] Olano L, Montero I. Energy spectra of secondary electrons in dielectric materials by charging analysis. Results Phys 2020;19:103456.
[13] Greenwood J. The correct and incorrect generation of a cosine distribution of scattered particles for Monte-Carlo modelling of vacuum systems. Vacuum 2002;674(2):217–22.
[14] Vaughan J. A new formula for secondary emission yield. IEEE Trans Electron Devices 1989;36(9):1963–7.
[15] Furman MA, Pivi MTF. Probabilistic model for the simulation of secondary electron emission. Phys Rev ST Accel Beams 2002;5:124404.
[16] de Lara J, Perez F, Alfonseca M, Galan L, Montero I, Roman E, et al. Multipactor prediction for on-board spacecraft RF equipment with the MEST software tool. IEEE Trans Plasma Sci 2006;34(2):476–84.
[17] Somersalo E, Yla-Oijala P, Sarvas J, Proch D. Computational methods for analyzing electron multipacting in rf structures. Part Accel 1998;59:107–41.
[18] Nanotec Co, https://www.nanotec-jp.com/.
[19] Grudiev A, Neupert H, Vollenberg W, Jing C, Poddar S, Freemire B. Amorphous and diamond-like carbon coatings for SEY reduction of dielectric materials for accelerating structure applications. CERN Report 2022.
[20] MATLAB. 2024, https://www.mathworks.com/products/matlab.html (Accessed March 2024).